

Fluctuating Filaments Under Tension - From Flexible Chains to Rigid Rods

David A. Kessler and Yitzhak Rabin

Department of Physics, Bar-Ilan University, Ramat-Gan 52900, Israel

(Dated: November 9, 2018)

We develop a novel biased Monte-Carlo simulation technique to measure the force-extension curves and the distribution function of the extension of fluctuating filaments stretched by external force. The method is applicable for arbitrary ratio of the persistence length to the contour length and for arbitrary forces. The simulation results agree with analytic expressions for the force-extension curves and for the renormalized length-scale-dependent elastic moduli, derived in the rigid rod and in the strong force limits. We find that orientational fluctuations and wall effects produce non-Gaussian distributions for nearly rigid filaments in the small to intermediate force regime. We compare our results to the predictions of previous investigators and propose new experiments on nearly rigid rods such as actin filaments.

PACS numbers: 87.15.Aa,87.15.Ya,05.40.-a

I. INTRODUCTION

Recent experimental studies of the mechanical properties of biological materials, ranging from individual DNA molecules[1] to single actin filaments and their networks[2, 3, 4], led to revival of interest in the worm-like chain model of semiflexible biopolymers. In particular, the force-extension curves predicted by this model in the long chain limit (i.e., when the length of the chain is much larger than the persistence length) were shown to agree quantitatively with experimental results on dsDNA at large elongations[5]. However, many interesting questions concerning worm-like chains under tension are still open and there are delicate issues concerning even the linear response of the worm-like chain to stretching force[6]. Also, while the equilibrium distribution function of the extension was calculated for the worm-like chain[7, 8, 9] and fluctuating ribbon[10] models, only approximate (using the Gaussian approximation) calculations of the distribution function for stretched chains were reported to date[11]. Such distributions have been measured in experiments on stretched DNA molecules[12] and provide a much more stringent test of the theory than the force-extension curves. Finally, even though all mechanical experiments involve biopolymers attached to surfaces, none of the present theories incorporates wall effects on force-extension curves and on the corresponding distributions. While such effects are negligible for nearly fully stretched chains, they are expected to be important in the weak force regime.

In previous work[10, 13], we have discussed how to generate via Monte-Carlo equilibrium ensembles of fluctuating ribbons with spontaneous curvature and/or twist. This method was based on using the intrinsic geometry of the filament, in which representation the energy is purely quadratic. This enables a direct generation of independent samples distributed according to the Gibbs equilibrium ensemble. When external forces act on the filaments, the energy is no longer a quadratic function of the curvatures, and the problem is now not only nonlinear but also nonlocal. In this paper we discuss a biasing method which succeeds in efficiently generating Monte-Carlo samples for the simplest case of an external force, namely that of the stretched filament. This problem was studied by Marko and Siggia, (MS), [5, 14] and others [15, 16] who calculated the force-extension curve for long worm-like chains. We will reproduce these results as well as extend the analysis to the case of nearly stiff filaments with length comparable to or shorter than the persistence length, and in addition calculate the distribution of extensions for various forces. Lastly, we will show how we can also easily incorporate steric constraints; we will demonstrate this in the context of a restriction of the filament to a half-space by the presence of a wall.

In sections 2 and 3 we review the general theory of fluctuating ribbons (we define a ribbon as a filament with an asymmetric cross-section) and the Frenet algorithm for computer simulations of such ribbons, respectively. In section 4 we describe the biased Monte-Carlo simulations of filaments under tension and present the resulting force-extension curves and distribution functions. Wall effects are considered in section 5. In section 6 we discuss our results and outline directions for future research. In Appendix A we expand the Euler angles in terms of the principal curvatures and then use this expansion in Appendix B in order to calculate the partition function of a stretched filament. In part 1 of this appendix we derive an analytic expression for the partition function and obtain a force-extension relation for arbitrary force in the limit of large persistence length (expansion about the rigid rod limit). In part 2 of the appendix we derive asymptotic expressions for the above quantities in the limit of large force (for arbitrary rigidity). Finally, in Appendix 3 we present the calculation of the renormalization of the elastic moduli of the various Fourier modes of the curvature.

II. GENERAL THEORY

The linear elasticity of ribbons is described by the elastic energy[17]

$$E_{el} = \frac{1}{2} \sum_{k=1}^3 b_k \int_0^L ds (\omega_k - \omega_{0k})^2, \quad (1)$$

where s is the distance measured along the contour of the ribbon, the coefficients b_1 and b_2 are the moduli associated with bending along the two principal axes of inertia of the cross section (they differ if the cross section is not circular), and b_3 is the twist modulus. In this paper we treat $\{b_i\}$ as given material parameters of the ribbon. The functions $\{\omega_k(s)\}$ and $\{\omega_{0k}(s)\}$ are the generalized curvatures in the deformed and the stress-free states of the ribbon, respectively. These curvatures completely determine the three dimensional conformation of the ribbon through the generalized Frenet equations[17]

$$\frac{d\mathbf{t}_i(s)}{ds} = - \sum_{j,k} \varepsilon_{ijk} \omega_j(s) \mathbf{t}_k(s). \quad (2)$$

Here \mathbf{t}_3 is the unit tangent to the centerline and the unit vectors \mathbf{t}_1 and \mathbf{t}_2 are oriented along the principal axes of the cross section (ε_{ijk} is the antisymmetric unit tensor). Note that since these equations describe a pure rotation of the triad $\{\mathbf{t}_i(s)\}$ as one moves along the contour of the ribbon, the constraint $|\mathbf{t}_3| = |d\mathbf{r}(s)/ds| = 1$ is automatically satisfied in this intrinsic coordinate description.

The physical frame of the ribbon $\{\mathbf{t}_i(s)\}$ can be related to the original Frenet description of space curves in terms of a unit tangent (which coincides with \mathbf{t}_3), normal \mathbf{n} and binormal \mathbf{b} , provided that in addition to the Frenet triad $\{\mathbf{b}(s), \mathbf{n}(s), \mathbf{t}_3(s)\}$ associated with the centerline of the ribbon, one introduces an angle $\alpha(s)$ that describes the rotation of two of the principal axes of the cross section $\mathbf{t}_1, \mathbf{t}_2$ with respect to the binormal \mathbf{b} and normal \mathbf{n} (see Fig. 1 in the second of Refs. [17]),

$$\mathbf{t}_1 = \mathbf{b} \cos \alpha + \mathbf{n} \sin \alpha, \quad \mathbf{t}_2 = -\mathbf{b} \sin \alpha + \mathbf{n} \cos \alpha. \quad (3)$$

The three dimensional configuration of the centerline is determined by the Frenet equations

$$\frac{d\mathbf{b}}{ds} = \tau \mathbf{n}, \quad \frac{d\mathbf{n}}{ds} = \kappa \mathbf{t}_3 - \tau \mathbf{b}, \quad \frac{d\mathbf{t}_3}{ds} = -\kappa \mathbf{n} \quad (4)$$

where the curvature $\kappa(s)$ and torsion $\tau(s)$ are treated as known functions of position along the contour. The three generalized curvatures $\{\omega_k(s)\}$, can be expressed in terms of these parameters and the angle $\alpha(s)$,

$$\omega_1 = \kappa \cos \alpha, \quad \omega_2 = \kappa \sin \alpha, \quad \omega_3 = \tau + d\alpha/ds. \quad (5)$$

III. THE FRENET ALGORITHM

Since the energy is a quadratic form in the deviations $\delta\omega_k$ of the generalized curvatures from their values in the stress free state, Eq. (1) is valid as long as the characteristic length scale of the deformation is much larger than the diameter of the ribbon[18]. When a ribbon undergoes fluctuations in the presence of a thermal bath at temperature T , this energy determines the statistical weight of the configuration $\{\omega_k\}$. The statistical average of any functional of the configuration $A(\{\omega_k\})$ is defined as the functional integral[17]

$$\langle A(\{\omega_i\}) \rangle = \frac{\int D\{\delta\omega_i\} A(\{\omega_i\}) e^{-E_{el}\{\delta\omega_i\}/kT}}{\int D\{\delta\omega_i\} e^{-E_{el}\{\delta\omega_i\}/kT}}. \quad (6)$$

where k is the Boltzmann constant. From the form of the energy, Eq. 1, it follows that the distribution of $\delta\omega_k$ is Gaussian, with zero mean ($\langle \delta\omega_i(s) \rangle = 0$) and second moments given by

$$\langle \delta\omega_i(s) \delta\omega_j(s') \rangle = \frac{kT}{b_i} \delta_{ij} \delta(s - s'). \quad (7)$$

In order to study the distribution functions of the various fluctuating quantities (e.g., the extension R), we developed what we entitled the Frenet algorithm, which is based on the combination of statistical methods and differential

geometry and is described in the following. Examination of Eq. (7) shows that the decoupling of the “noises” $\{\delta\omega_k\}$ in the intrinsic coordinate representation permits an efficient numerical generation of independent samples drawn from the exact canonical distribution. The Gaussian distribution of the $\delta\omega_k$ means that each $\delta\omega_k(s)$ can be directly generated as one of a string of independent random numbers drawn from a distribution symmetric about the origin with width $\sqrt{kT/(b_k\Delta s)}$ where Δs is the discretization step length. The remaining task is to construct the curve using the Frenet equations with $\omega_k(s) = \omega_{0k}(s) + \delta\omega_k(s)$. The Frenet equations are best integrated by stepping the basic triad t_k forward in s through a suitable small rotation. In this way, the orthonormality of the triad is guaranteed to be preserved up to machine accuracy. To construct this rotation matrix, we begin with Eqs. (2) and, defining the three vectors $v^x = (t_1^x, t_2^x, t_3^x)$, and so forth, we can write this equation as

$$\frac{\Delta v^i}{\Delta s} = Av^i, \quad (8)$$

where A is an antisymmetric matrix with elements $A_{ij} = \sum_k \varepsilon_{ijk}\omega_k$. We now discretize Eq. (8) as

$$v^i(s + \Delta s) = Ov^i(s), \quad (9)$$

where the orthogonal matrix O is

$$O = \left(1 + \frac{\Delta s}{2}A\right) \left(1 - \frac{\Delta s}{2}A\right)^{-1}. \quad (10)$$

The choice of discretization step length ($L/\Delta s$ is the number of points) depends on the amplitude of the random noise, $\sqrt{kT/(b_k\Delta s)}$. We found that 400 points gave sufficient accuracy (i.e., was limited by the statistical noise determined by the number of independent samples) for the calculation of the distribution function of the extension, when the smallest of the moduli satisfied $kTL/b_k^{\min} \lesssim 1$.

This algorithm is optimal for studying the fluctuations of a free ribbon. However, if the ribbon is acted upon by external forces and/or constraints, the algorithm must be modified. This is described in the next section.

IV. BIASING THE MONTE-CARLO

Consider a filament with a circular cross-section ($b_1 = b_2$) which is characterized by a bending persistence length

$$a = \frac{b_1}{kT}. \quad (11)$$

The simplest example of a filament under tension is that of a constant force acting on one end and directed along the x -axis, with the second end constrained to lie at the origin but otherwise free to rotate about it. The energy of the filament thus picks up an additional contribution $-Fx$, where x is the projection of the end to end vector on the direction of the force. The problem is that x is a complicated nonlinear function of all the $\delta\omega$, and so the external force destroys the Gaussian structure of the energy on which the generation of the $\delta\omega$ depends. One can simply incorporate the extra contribution to the energy by treating it as a weighting factor, or bias, and suitably normalizing all averages. Thus, for example, one can calculate the mean value of x via

$$\bar{x} = \frac{\sum x e^{fx}}{\sum e^{fx}} \quad (12)$$

where the sum is over configurations generated via the Frenet algorithm described above and $f \equiv F/kT$ is the force in units of inverse length. For small forces, this works well. However, as the force increases, the probability of generating highly extended configurations which are heavily favored by the bias, is so small that the sampling becomes ineffective. One therefore needs a way to bias the generation of configurations towards those that are extended, so they can be sampled appropriately.

This task is not simple, since the connection between the $\delta\omega$'s through which the filament is parameterized and the value of x is very complicated. We can gain insight into this by transforming to Fourier space and looking at the expectation value of the moments of the n 'th Fourier component of the curvature, $\delta\tilde{\omega}(n)$, using the above algorithm, Eq. 12, for small to intermediate forces where it is still effective. For an extensional force, we do not expect spontaneous curvature to develop, and indeed the first moments of the Fourier components all vanish. The second moments, however, do exhibit an interesting structure, as seen in Fig. 1, where the expectation value of the squared amplitude of the low n Fourier modes are presented for the case $a = 3$, $L = 2\pi$. For $F = 0$, the

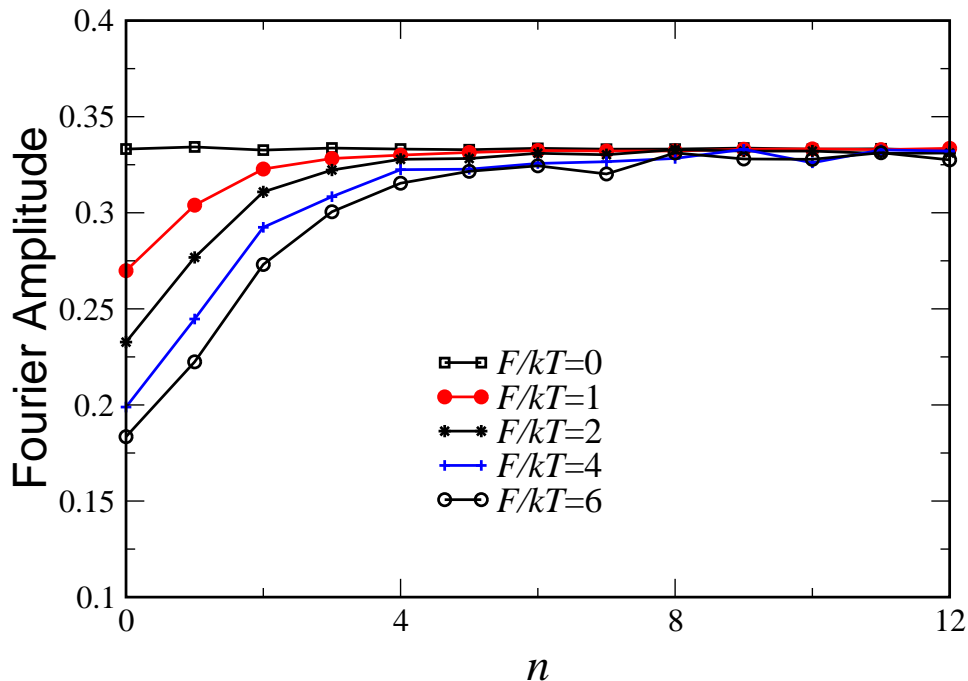


FIG. 1: Amplitude of Fourier components of the curvature, as a function of mode number n for different forces F/kT , for $L = 2\pi$, $a = 3$. The lines are added to guide the eye.

second moments are independent of n , as expected. When the filament is subjected to a tensile force we see that the small n modes are suppressed, with the degree of suppression increasing with F and decreasing with n . In the case of large a , where the fluctuations are in any case small, we observe that only the $n = 0$ mode is significantly affected by the force (not shown). The suppression of the various curvature modes can be calculated analytically when fluctuations are small, namely either in the large FL limit, or for any F provided $\chi \equiv \sqrt{FL^2/(4akT)} \ll 1$ (see Appendix). The calculation confirms the above-mentioned trends. We learn from this that the high Fourier modes (or equivalently the small-scale fluctuations) of the filament are essentially unaffected by the force, whereas the long-wavelength fluctuations are significantly damped.

This suggests the possibility of biasing the Monte-Carlo by selectively dampening the small- n modes. The idea is to generate the $\delta\tilde{\omega}$'s in Fourier space, with appropriate amplitudes for the various modes, and construct the real-space $\delta\omega(s)$ via a Fast Fourier Transform. Of course, this bias has to be corrected explicitly in the weighting in the ensemble average. We do this in a self-consistent fashion, choosing the amplitude of each Fourier mode to reproduce the measured square magnitude of the mode. In practice, it is sufficient to do this only for the first few modes, which are the ones most severely impacted by the force. Also, in order to reduce the noise in the measurement of the mode amplitudes, we only calculate the averages after every block of $N/10$ realizations and update accordingly, where N is the total number of realizations we intend to generate for these parameters. The force dependence of the mode amplitudes is obtained by a stepwise increase of F , where for each value of the force we use as a starting point the amplitudes measured at the previous value.

There is one other degree of freedom of the problem that also must be treated appropriately, namely the initial orientation of the filament at its constrained end. This is because the force not only straightens the filament, but also orients it toward its direction. We have employed two different algorithms to deal with this problem. The simpler approach is to simply bias the choice of initial orientation, and correct for this in the weighting. The zero force distribution of the orientation angle, θ , of the tangent vector with respect to the direction of the force is $P(\theta) = \sin\theta d\theta = d(\cos\theta)$. In the presence of the force we modified this to $P(\cos\theta) = \exp(\alpha \cos\theta) d(\cos\theta)$, where one can choose α to reproduce the measured mean of $\cos\theta$.

A more sophisticated approach is to explicitly perform the integral over θ . We generate a given configuration and calculate its end-to-end distance R and angle θ_{end} that the tangent to the end of the filament makes with the direction of the end-to-end vector \mathbf{R} . In order to evaluate the contribution of this realization to the average elongation, Eq. 12, one can perform a rigid rotation of this configuration about the end point and calculate the contribution to the statistical sum, from each angle of rotation θ . The resulting integrals over θ can be expressed in terms of R and θ_{end}

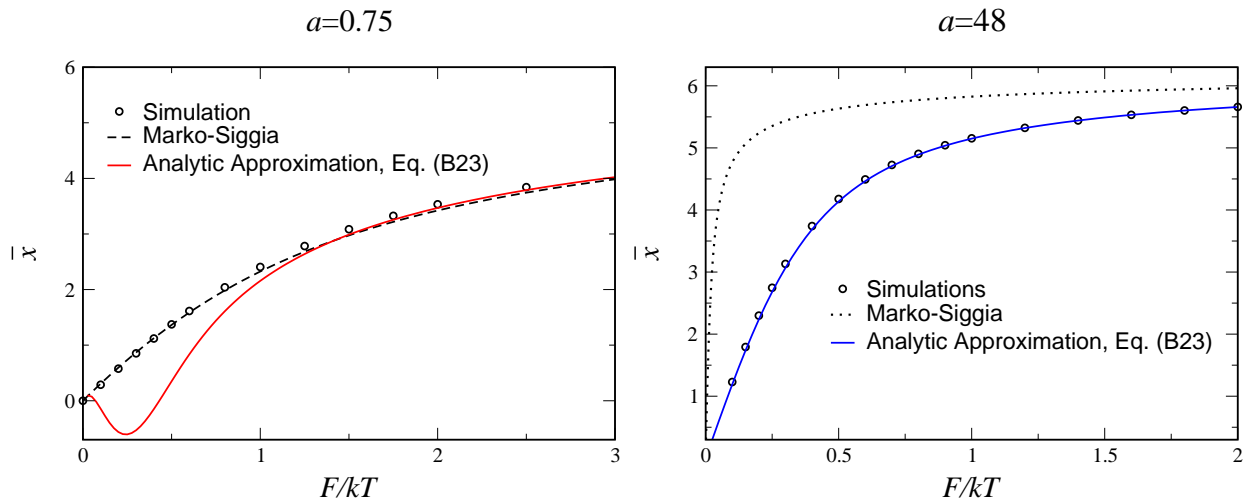


FIG. 2: Extension along the force direction of a filament, as measured by our Monte-Carlo procedure, together with the Marko-Siggia interpolation formula and our analytic approximation, Eq. (B23) for $L = 2\pi$. Left: $a = 0.75$; Right: $a = 48$.

as

$$\int_0^\pi d\theta \sin\theta \{R \cos(\theta + \theta_{end}), 1\} e^{f R \cos(\theta + \theta_{end})} \quad (13)$$

where the curly braces indicate the integrand for the numerator and denominator of the ensemble sum, respectively. These integrals can easily be evaluated numerically, using standard techniques. This second method is more efficient, but more involved to implement.

Using these techniques, we have measured the force-extension curve \bar{x} vs. f . We present the results for $a = .75$, $L = 2\pi$ in the left box of Fig. 2 together with the interpolation formula of MS

$$fa = \frac{\bar{x}}{L} + \frac{1}{4(1 - \bar{x}/L)^2} - \frac{1}{4} \quad (14)$$

We see that for this value of a ($a \ll L$) the agreement is very good. In the right half of Fig. 2 we present the results for $a = 48$, again with $L = 2\pi$. Here the MS formula does not work for small and intermediate values of the force, since we are not in the long-chain limit ($L \gg a$) for which it was derived. On the other hand, for this case analysis can also be done, as presented in the Appendix, and the analytic formula derived there is in perfect agreement with the simulations (see the right box of Fig. 2). Notice that the MS expression systematically overestimates the extension of the filament and approaches our results only in the infinite force limit. The physical basis of the deviation is the large orientational entropy which is not accounted for in the MS calculation.

Inspection of the right box of Fig. 2 suggests that both the simulation and our analytical approximation (Eq. B12) yield a finite initial slope of the extension versus force curve in the rigid rod limit ($a \gg L$). Since the effective spring constant is proportional to the inverse of the initial slope of this curve this suggests that the linear response of the rigid rod to small stretching forces does not depend on the persistence length a and is a function of its length L only. The above expectation is confirmed by calculations reported in Appendix B where we show that the corresponding spring constant is $3kT/L^2$. Obviously, this behavior differs from the flexible chain limit ($a \ll L$) for which the spring constant scales as [19] $kT/(aL)$. It also differs from the predictions of Ref. [6] where it was argued that the effective spring constant diverges in the rigid rod limit, as akT/L^3 . Notice that such a divergence is not expected for a single filament under tension since there is a finite contribution to the susceptibility (and thus to the response to the external force) due to orientational fluctuations, even in the rigid rod limit. The difference between our result and that of Ref. [6] stems from the fact that the latter considers a network in which filaments are not free to rotate and the only angular averaging is over the randomly distributed orientations of different filaments in the network.

Not only can we calculate the average \bar{x} , but we can also measure the entire distribution $P(x)$. We show this in Fig. 3, for $a = 0.75$ and 6. In the former case, the persistence length is much shorter than length of the filament and the force-free distribution is nearly Gaussian. The peak of the distribution moves to higher values of the extension and its width decreases with increasing force. In the latter case (persistence length approximately equal to the length of the filament), the force-free distribution is nearly flat up to $x \simeq \pm 5$, as expected for random sampling of orientations by

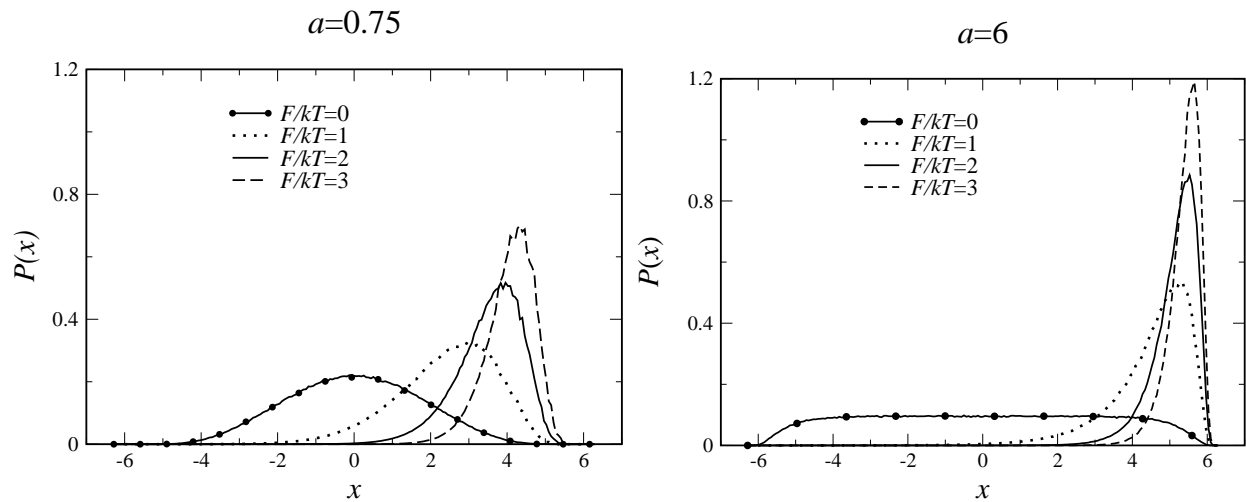


FIG. 3: Distribution of the extension along the force direction, as measured by our Monte-Carlo procedure, for the cases $f = 0, 1, 2$ and 3 , with $L = 2\pi$. Left: $a = 0.75$; Right: $a = 6$.

a nearly rigid rod (due to thermal fluctuations, the effective length of this rod is somewhat shorter than its contour length, 2π). The application of small force (in the range $F/kT \leq 1$) orients the filament and leads to dramatic change of the distribution. At larger forces, the distribution changes slowly with the force, in a manner similar to the case $a = 0.75$. The transition from orientation-dominated to stretching-dominated behavior of nearly rigid rods is clearly observed in the right box of Fig. 2, where pronounced deviations from the Marko-Siggia formula are observed in the weak force regime (orientational effects are not taken into account in the MS theory).

V. STERIC CONSTRAINTS

It is fairly straightforward to incorporate steric constraints into our calculations. As an example, we consider the case where the filament is confined to the upper half space $x > 0$. After generating each configuration according to the procedure outlined in the previous section, we simply reject any configuration which violates the constraint. Our method of integrating over the initial orientation angle θ can also be employed. We have simply to compute the limits of the integral over θ which can be done straightforwardly given the configuration. We present the results for the force-extension curve in Fig. 4 and for the distribution $P(x)$ in Fig. 5. We see that, as one might expect, the effect of the constraint is most pronounced at small F , where the straightening/aligning of the curve is smallest. For vanishing F , the average extension is positive as a result of the constraint. The constraint basically carves out a “hole” in the distribution at small x , resulting in a very asymmetric distribution for small force. For $F/kT > 1$ the distribution function is practically unaffected by the presence of the wall and coincides with that shown in Fig. 3.

VI. DISCUSSION

In this work we used biased Monte-Carlo simulations, based on an extension of our Frenet algorithm, to calculate the force-extension relations and the distribution functions of the extension for filaments of arbitrary persistence to contour length ratio. We showed that in the presence of external force, curvature fluctuations are no longer Gaussian and that their long wavelength Fourier modes are progressively suppressed by the force. This effect was taken into account in a self-consistent manner in the simulations by gradually increasing the force and adjusting the corresponding Fourier amplitudes of curvature fluctuations. Analytic results were obtained both for small fluctuations about the rigid rod limit, and in the limit of large force. In the former case, we calculated the force-induced renormalization of the length-scale-dependent bending moduli that govern the various Fourier modes of curvature. As expected, the largest effect is on the zeroth (constant curvature) mode; the corresponding modulus increases quadratically and linearly with the force in the weak and strong force limits, respectively. The underlying physical picture is reminiscent of the suppression of excluded volume by tensile force in the self-avoiding random walk model of polymers - while large scale fluctuations are strongly suppressed, small scale fluctuations (within the so called Pincus blobs[20]) are not affected by the force.

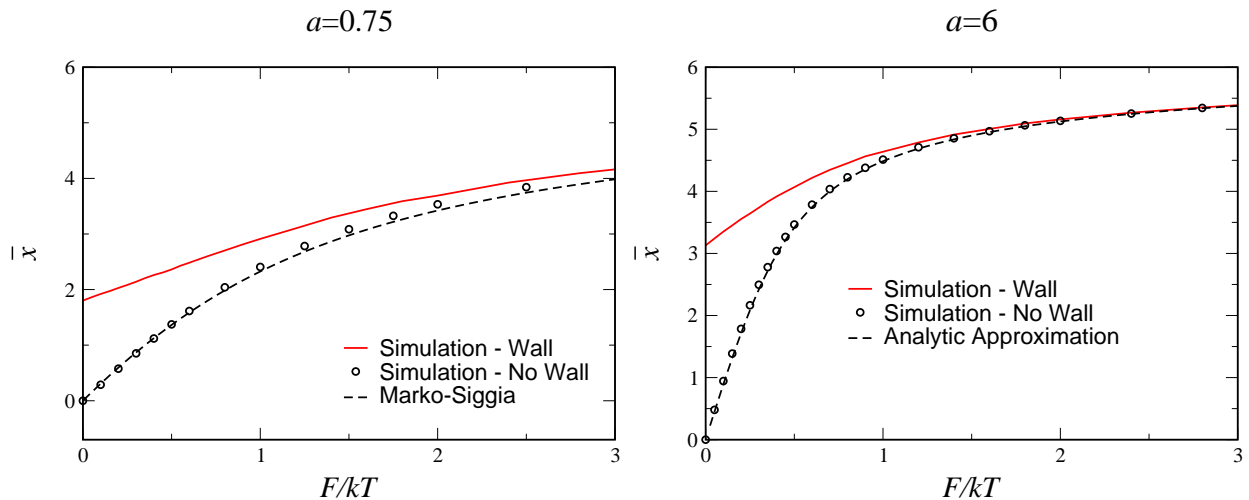


FIG. 4: Force-extension curve with and without the presence of a wall confining the filament to $x > 0$ for $L = 2\pi$, measured via our Monte-Carlo procedure. Left: $a = 0.75$, together with the Marko-Siggia formula; Right: $a = 6$, together with our formula, Eq. (B23).

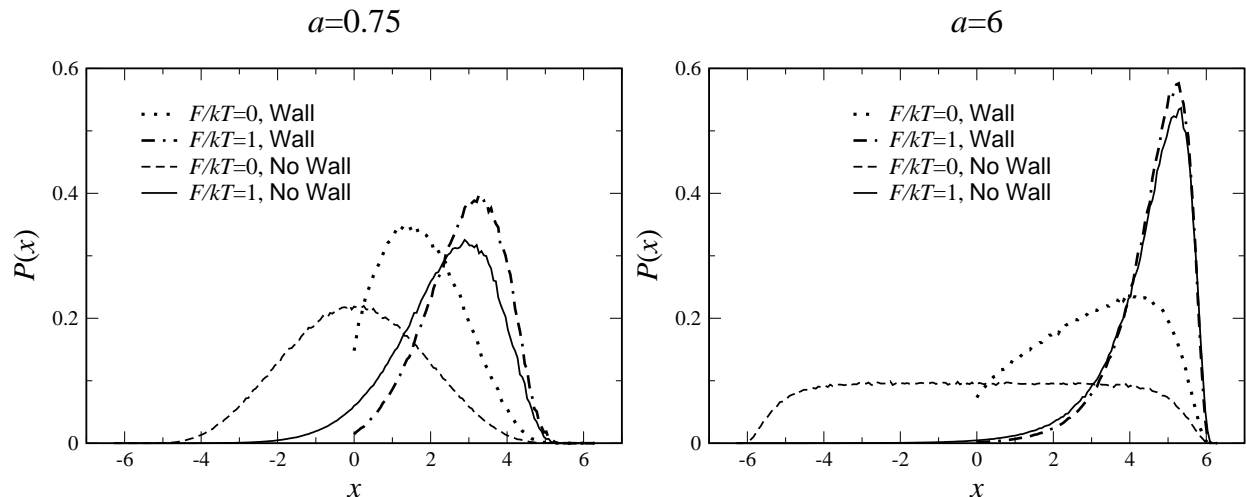


FIG. 5: Distribution of the extension along the force direction with and without the constraining wall, for $f = 0, 1$, with $L = 2\pi$. Left: $a = 0.75$; Right: $a = 6$. Distributions at higher forces are essentially unaffected by the constraint.

For flexible filaments with $a \ll L$ our simulation reproduces the Marko-Siggia force-extension curves. However, our simulations and analytic results show that as the rigid rod limit $a \gg L$ is approached, the MS expression increasingly overestimates the response of the filament at finite values of the force, and approaches the correct result only asymptotically, in the limit of infinite force. The discrepancy can be attributed to the neglect of orientational effects (the constant curvature mode is not taken into account) in the MS derivation which is strictly valid only in the $a/L \rightarrow 0$ limit. These orientational effects are however seen in the short-chain limit of the Gaussian model investigated recently by Winkler[11]. The large force limit of the Gaussian model for short chains is however very different from the worm-like chain model studied herein. For long chains, the Gaussian model can reproduce either the weak or the strong force limit, by appropriate choice of the persistence length, but not both. This is an outcome of the length-scale dependence of the effective moduli discussed above and in Appendix C.

Examination of the distribution functions for the extension shows that increasing rigidity leads to a more rapid shift of the peak of the distribution and narrowing of its width, with external force. The largest deviations from Gaussian statistics of the distributions are observed for stiff filaments in the weak to intermediate force range ($F/kT \leq 1$), where fluctuations of initial orientation are not yet completely suppressed and where wall effects play an important role. While it may be difficult to approach the rigid rod limit in mechanical experiments on dsDNA that has a persistence length of 500 Å, it can be readily accessed by experiments on actin filaments[2] for which the persistence length of

order $10 \mu\text{m}$.

Finally, we would like to comment on possible extensions of the present work. Since we only considered here filaments with symmetric cross section and without spontaneous curvature, twist rigidity did not affect the distribution of extension and played no role in our considerations. However, since twist rigidity affects even the equilibrium distributions of ribbons with strongly asymmetric cross sections[10], it is expected that both twist rigidity and spontaneous twist will affect the deformation of such ribbons as well. Perhaps even more interesting is the effect of spontaneous curvature. Indeed, we have shown that a helical filament with sufficiently large twist to bending rigidity and radius to pitch ratios, undergoes a sequence of stretching instabilities under the action of tensile force, even in the absence of any thermal fluctuations[22]. In the presence of thermal fluctuations or mechanical noise these instabilities are expected to lead to coexistence between different shapes of the deformed object[23].

Acknowledgments

DAK and YR acknowledge the support of the Israel Science Foundation. We also would like to thank J. Fineberg and G. Cohen for stimulating discussions.

APPENDIX A: EULER ANGLES

Since we are interested in three dimensions, we work in terms of the Euler angles θ , ϕ and ψ . For convenience we will orient the force along the x -axis, i.e. along the direction $\theta = \pi/2$, $\phi = 0$. The energy due to the force is then

$$E_F = -Fx = -F \int_0^L ds t_3^x = -F \int_0^L ds \sin(\theta(s)) \cos(\phi(s)) \quad (\text{A1})$$

The Euler angles satisfy the differential equations[21]:

$$\begin{aligned} \frac{d\theta}{ds} &= \omega_1 \sin \psi + \omega_2 \cos \psi \\ \frac{d\phi}{ds} \sin \theta &= -\omega_1 \cos \psi + \omega_2 \sin \psi \\ \frac{d\psi}{ds} \sin \theta &= (\omega_1 \cos \psi - \omega_2 \sin \phi) \cos \theta + \omega_3 \sin \theta \end{aligned} \quad (\text{A2})$$

We need to expand to quadratic order about the $s = 0$ values θ_0 and ϕ_0 , and to linear order about ψ_0 , (since the energy does not involve ψ directly) giving

$$\begin{aligned} \frac{d\theta}{ds} &= \kappa - \lambda(\psi - \psi_0), \\ \frac{d\phi}{ds} &= \frac{\lambda + \kappa(\psi - \psi_0)}{\sin \theta_0} - \frac{\cos \theta_0}{\sin^2 \theta_0} \lambda(\theta - \theta_0), \\ \frac{d\psi}{ds} &= -\frac{\cos \theta_0}{\sin \theta_0} \lambda + \omega_3, \end{aligned} \quad (\text{A3})$$

where κ and λ are the rotated curvatures

$$\begin{aligned} \kappa &\equiv \omega_1 \sin \psi_0 + \omega_2 \cos \psi_0, \\ \lambda &\equiv -\omega_1 \cos \psi_0 + \omega_2 \sin \psi_0, \end{aligned} \quad (\text{A4})$$

Thus, to second order in the curvatures

$$\begin{aligned} \theta(s) &= \theta_0 + \int_0^s ds' \kappa(s') + \frac{\cos \theta_0}{2 \sin \theta_0} \left(\int_0^s ds' \lambda(s') \right)^2 - \int_0^s ds' \lambda(s') \int_0^{s'} ds'' \omega_3(s''), \\ \phi(s) &= \phi_0 + \frac{1}{\sin \theta_0} \int_0^s ds' \lambda(s') - \frac{\cos \theta_0}{\sin^2 \theta_0} \left(\int_0^s ds' \kappa(s') \right) \left(\int_0^s ds' \lambda(s') \right) \\ &\quad + \frac{1}{\sin \theta_0} \int_0^s ds' \kappa(s') \int_0^{s'} ds'' \omega_3(s''). \end{aligned} \quad (\text{A5})$$

APPENDIX B: FORCE-EXTENSION CURVE

We will first compute the force-extension curve, via the partition function. We do this in two stages, depending on the value of the parameter $\chi \equiv \sqrt{FL^2/4a}$.

1. Small χ ($\chi \ll 1$, arbitrary fL)

Here we write

$$E_F = -FL \sin \theta_0 \cos \phi_0 + F\delta \quad (\text{B1})$$

where δ is given by

$$\begin{aligned} \delta = - \int_0^L ds & \left[\cos \theta_0 \cos \phi_0 \int_0^s \kappa - \sin \phi_0 \int_0^s \lambda - \frac{1}{2} \sin \theta_0 \cos \phi_0 \left[\left(\int_0^s \kappa \right)^2 + \left(\int_0^s \lambda \right)^2 \right] \right. \\ & \left. - \cos \theta_0 \cos \phi_0 \int_0^s ds' \lambda(s') \int_0^{s'} \omega_3 - \sin \phi_0 \int_0^s ds' \kappa(s') \int_0^{s'} \omega_3 \right] \end{aligned} \quad (\text{B2})$$

We expand $e^{-F\delta/kT}$ to quadratic order, yielding

$$\begin{aligned} Z = \int d\Omega_0 \mathcal{D}\kappa \mathcal{D}\lambda \exp & \left[-\frac{a}{2} \int_0^L (\kappa^2 + \lambda^2) + fL \sin \theta_0 \cos \phi_0 \right] \\ & \times \left[1 - f\delta + \frac{f^2}{2} \delta^2 \right] \end{aligned} \quad (\text{B3})$$

where $\int d\Omega_0 \equiv \frac{1}{4\pi} \int_0^\pi \sin \theta_0 d\theta_0 \int_0^{2\pi} d\phi_0$. The functional integrals are all Gaussian and can be easily done by going to Fourier space. For example,

$$\kappa(s) = \kappa_0 + \sum_{n=1}^{\infty} \kappa_n^c \cos\left(\frac{2\pi ns}{L}\right) + \sum_{n=1}^{\infty} \kappa_n^s \sin\left(\frac{2\pi ns}{L}\right) \quad (\text{B4})$$

so that

$$\int_0^L \left(\int_0^s ds' \kappa \right)^2 ds = \frac{L^3}{3} \kappa_0^2 + L^3 \sum_{n=1}^{\infty} \frac{(\kappa_n^c)^2 + 3(\kappa_n^s)^2}{2(2\pi n)^2} + \text{mixed terms} \quad (\text{B5})$$

where the mixed terms will vanish later upon functional integration and are omitted in the following. Defining

$$\mathcal{D}_0\kappa \equiv \mathcal{D}\kappa e^{-\frac{a}{2} \int_0^L \kappa^2 ds} = \mathcal{D}\kappa e^{-\frac{aL}{2} \kappa_0^2 - \frac{aL}{4} \sum_{n=1}^{\infty} ((\kappa_n^c)^2 + (\kappa_n^s)^2)} \quad (\text{B6})$$

and carrying out the functional integration by integrating over all the Fourier components

$$\mathcal{D}\kappa \equiv d\kappa_0 \prod_{i=1}^{\infty} d\kappa_i^c \prod_{j=1}^{\infty} d\kappa_j^s, \quad (\text{B7})$$

we get

$$\int \mathcal{D}_0\kappa \int_0^L \left(\int_0^s ds' \kappa \right)^2 ds = \mathcal{N} \frac{L^2}{2a} \quad (\text{B8})$$

where $\mathcal{N} = \int \mathcal{D}_0\kappa$ is the (normalization) integral over the exponential factor only. Similarly,

$$\int \mathcal{D}_0\kappa \left[\int_0^L \left(\int_0^s \kappa \right) ds \right]^2 = \int \mathcal{D}_0\kappa \left[\frac{\kappa_0 L^2}{2} + \sum_{n=1}^{\infty} \frac{\kappa_n^s L^2}{2\pi n} \right]^2 = \mathcal{N} \frac{L^3}{3a}.$$

The functional integration with respect to λ is carried out in the same manner. Putting this all together, we get

$$Z = \mathcal{N}^2 \int d\Omega_0 e^{fL \sin \theta_0 \cos \phi_0} \left[1 - \frac{fL^2}{2a} \sin \theta_0 \cos \phi_0 + \frac{f^2 L^3}{6a} (\cos^2 \theta_0 \cos^2 \phi_0 + \sin^2 \phi_0) \right] \quad (\text{B9})$$

The integrals over solid angle are as follows:

$$\begin{aligned} \int d\Omega_0 e^{fL \sin \theta_0 \cos \phi_0} &= \frac{\sinh fL}{fL} \\ \int d\Omega_0 e^{fL \sin \theta_0 \cos \phi_0} \sin \theta_0 \cos \phi_0 &= \frac{\cosh fL}{fL} - \frac{\sinh fL}{(fL)^2} \\ \int d\Omega_0 e^{fL \sin \theta_0 \cos \phi_0} \cos^2 \theta_0 \cos^2 \phi_0 &= \frac{1 + \cosh fL}{(fL)^2} - \frac{2 \sinh fL}{(fL)^3} \\ \int d\Omega_0 e^{fL \sin \theta_0 \cos \phi_0} \sin^2 \phi_0 &= \frac{\cosh fL - 1}{(fL)^2} \end{aligned} \quad (\text{B10})$$

Collecting all terms we finally get

$$Z = \mathcal{N}^2 \left\{ \frac{\sinh fL}{fL} - \frac{L}{6a} \left[\cosh fL - \frac{\sinh fL}{fL} \right] \right\} \quad (\text{B11})$$

From this, we can differentiate to get the average projection of the end-to-end vector on the x -axis, $\bar{x} = d(\ln Z)/df$

$$\bar{x} = \frac{L}{\tanh fL} - \frac{1}{f} - \frac{2\chi^2}{3f} \left[\frac{1}{\tanh fL} - \frac{fL}{\sinh^2 fL} \right] \quad (\text{B12})$$

At large fL (but still small χ), this goes as $L - L^2/(6a) - 1/f$. For small fL this projection goes linearly with f as $\bar{x} \approx fL^2/3(1 - L/(3a))$ and we conclude that in the limit $a \gg L$ the effective ‘‘spring constant’’ is $3kT/L^2$.

2. Large fL (arbitrary χ)

We start by expanding θ_0, ϕ_0 about the values θ_0^*, ϕ_0^* which minimize E_F . To lowest order,

$$\begin{aligned} \theta_0^* &= \frac{\pi}{2} - \frac{1}{L} \int_0^L ds \int_0^s ds' \kappa \\ \phi_0^* &= -\frac{1}{L} \int_0^L ds \int_0^s ds' \lambda \end{aligned} \quad (\text{B13})$$

so that the expansion reads

$$\begin{aligned} E_F &= -FL - \frac{F}{2L} \left[\left(\int_0^L ds \int_0^s ds' \kappa \right)^2 + \left(\int_0^L ds \int_0^s ds' \lambda \right)^2 \right] + \frac{FL}{2} [(\theta_0 - \theta_0^*)^2 + (\phi_0 - \phi_0^*)^2] \\ &+ \frac{F}{2} \int_0^L ds \left[\left(\int_0^s ds' \kappa \right)^2 + \left(\int_0^s ds' \lambda \right)^2 \right] \end{aligned} \quad (\text{B14})$$

Let us now consider the functional integral over κ , the integral over λ being exactly the same. We have

$$\begin{aligned} Z_\kappa &= \int \mathcal{D}\kappa e^{-\frac{a}{2} \int_0^L ds \kappa^2 - \frac{f}{2} \int_0^L ds \left(\int_0^s ds' \kappa \right)^2 + \frac{f}{2L} \left[\int_0^L ds \int_0^s ds' \kappa \right]^2} \\ &= \int \mathcal{D}\kappa \exp \left\{ -\frac{aL}{2} \kappa_0^2 - \frac{aL}{4} \sum_{n=1}^{\infty} ((\kappa_n^c)^2 + (\kappa_n^s)^2) \right. \\ &\quad \left. - \frac{fL^3}{2} \left[\frac{\kappa_0^2}{12} + \sum_{n=1}^{\infty} \left(\frac{(\kappa_n^c)^2}{2(2\pi n)^2} + \frac{(\kappa_n^s)^2}{2(2\pi n)^2} - \frac{2\kappa_0 \kappa_n^c}{(2\pi n)^2} \right) \right] \right\} \end{aligned} \quad (\text{B15})$$

We can diagonalize this expression by shifting κ_n^c , defining

$$C_n \equiv \kappa_n^c - \frac{b_n}{a_n} \kappa_0 \quad (\text{B16})$$

with

$$a_n \equiv \frac{aL + b_n}{2}; \quad b_n \equiv \frac{fL^3}{(2\pi n)^2} \quad (\text{B17})$$

yielding an effective modulus of the zero mode

$$a_0 = a + \frac{fL^2}{12} - \sum_{n=1}^{\infty} \frac{b_n^2}{a_n} = \frac{a\chi}{\tanh \chi} \quad (\text{B18})$$

We can now calculate Z_κ :

$$\begin{aligned} Z_\kappa/Z_{\kappa,0} &= (a_0/a)^{-1/2} \prod_{n=1}^{\infty} \frac{aL}{2a_n} \\ &= (a_0/a)^{-1/2} \prod_{n=1}^{\infty} \left(1 + \frac{\chi^2}{(\pi n)^2}\right)^{-1} \\ &= (a_0/a)^{-1/2} \frac{\chi}{\sinh \chi} \\ &= \left[\frac{2\chi}{\sinh 2\chi}\right]^{1/2} \end{aligned} \quad (\text{B19})$$

where $Z_{\kappa,0}$ is the κ partition function at $f = 0$. The entire partition function is then

$$Z = \mathcal{N}^2 \frac{e^{fL}}{2fL} \frac{2\chi}{\sinh 2\chi} \quad (\text{B20})$$

For small χ , this yields

$$Z \approx \mathcal{N}^2 \frac{e^{fL}}{2fL} \left(1 - \frac{2\chi^2}{3}\right), \quad (\text{B21})$$

which agrees precisely with the large f expansion of Eq. (B11).

The average extension in this second region ($fL \gg 1$) is given by

$$\bar{x} = L - \frac{1}{2f} - \frac{\chi}{f \tanh 2\chi} \quad (\text{B22})$$

which for small χ gives $\bar{x} \approx L - 1/f - L^2/(6a)$, in accord with the large fL limit of the first region ($\chi \ll 1$). At large fL , it agrees with the Marko–Siggia result, Eq. (14). A uniform approximation for the force-extension relation is then

$$\bar{x} \approx -\frac{1}{2f} - \frac{\chi}{f \tanh 2\chi} + \frac{L}{\tanh fL} - \frac{2\chi^2}{3f} \left(\frac{1}{\tanh fL} - \frac{fL}{\sinh^2 fL} - 1\right). \quad (\text{B23})$$

This result is confirmed by simulations, as shown in data for $a = 48$, Fig. 2. It even works well when the persistence length slightly shorter than the chain length, as can be seen in the data for $a = 6$ in the right half of Fig. 4. Since our analysis is limited to the small fluctuation (stiff rod and/or large force) regime, we expect it to break down for very short persistence lengths in the small force limit. This is clearly observed in the case of $a = 0.75$, shown in the left half of Fig. 2.

APPENDIX C: MODULI

We now turn to the computation of the effective moduli of the various modes. We first treat the zero modes, starting as above with the small χ limit. We proceed by calculating a modified partition function, \tilde{Z} with a modified modulus of the zero modes, \tilde{a} , replacing the bare modulus a . Then

$$\frac{L}{2} \langle \kappa_0^2 + \lambda_0^2 \rangle = - \left. \frac{d \ln \tilde{Z}}{d \tilde{a}} \right|_{\tilde{a}=a} \quad (\text{C1})$$

Tracking the changes induced in the partition function calculation above, we find

$$\tilde{Z} = \frac{a}{\tilde{a}} \mathcal{N}^2 \left\{ \frac{\sinh fL}{fL} - fL^2 \left[\left(\frac{1}{3\tilde{a}} + \frac{1}{6a} \right) - \left(\frac{1}{4\tilde{a}} + \frac{1}{12a} \right) \right] \left[\frac{\cosh fL}{fL} - \frac{\sinh fL}{(fL)^2} \right] \right\} \quad (\text{C2})$$

giving

$$\ln \tilde{Z} = \ln a - \ln \tilde{a} + 2 \ln \mathcal{N} + \ln \frac{\sinh fL}{fL} - fL^2 \left(\frac{1}{12\tilde{a}} + \frac{1}{24a} \right) \left(\frac{\cosh fL}{\sinh fL} - \frac{1}{fL} \right) \quad (\text{C3})$$

so that

$$\left. \frac{d \ln \tilde{Z}}{d \tilde{a}} \right|_a = -\frac{1}{a} + \frac{fL^2}{12a^2} \left[\frac{\cosh fL}{\sinh fL} - \frac{1}{fL} \right] \quad (\text{C4})$$

This implies an effective zero mode modulus of

$$a_0 = a + \frac{fL^2}{12a} \left(\frac{1}{\tanh fL} - \frac{1}{fL} \right) \quad (\text{C5})$$

At small and large forces, this reads

$$a_0 \approx \begin{cases} a + f^2 L^3 / (36a) & fL \ll 1 \\ a + fL^2 / (12a) & fL \gg 1 \end{cases} \quad (\text{C6})$$

At large f , the effective zero mode modulus was calculated above, Eq. (B18). The small χ limit of this agrees with the large force limit of Eq. (C6), as it must. A uniform approximation for a_0 reads

$$a_0 = \frac{fL^2}{12a} \left(\frac{e^{-fL}}{\sinh fL} - \frac{1}{fL} \right) + a \frac{\chi}{\tanh \chi} \quad (\text{C7})$$

This result is confirmed by the simulations as seen in Fig. 6.

Now we turn to the finite wave-number modes. The interesting thing to note here is that the *cos* modes renormalize differently than the *sin* modes, due to the coupling of the zero mode to the *cos* modes. At large force, the effective modulus of the *sin* modes is the trivial

$$a_n^s = a + \frac{fL^2}{(2\pi n)^2} \quad (\text{C8})$$

so that the long wavelength modes are the most effected by the force. The effective modulus of the *cos* modes follows from

$$\langle (\kappa_n^c)^2 \rangle = \langle C_n^2 \rangle + \frac{b_n^2}{a_n^2} \langle \kappa_0^2 \rangle = \frac{1}{a_n} + \frac{b_n^2}{a_n^2} \frac{1}{a_{\text{eff},0} L} \quad (\text{C9})$$

with

$$a_n^c = \frac{2}{L \langle (\kappa_n^c)^2 \rangle} \quad (\text{C10})$$

This expression is fairly messy, so let us examine its various limits. For large enough mode number, the effective modulus is $a + fL^2 / (2\pi n)^2$ as for the *sin* modes. For intermediate forces, all modes are large enough for this to be

$$L=6.283, a=48$$

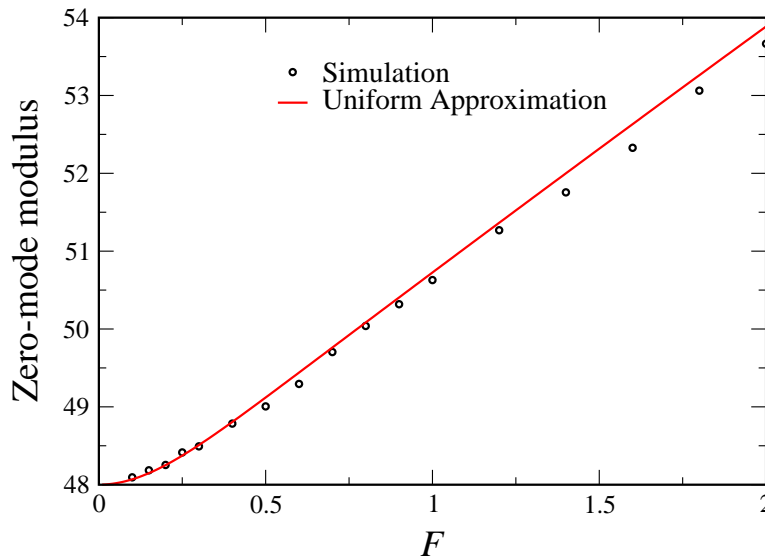


FIG. 6: Comparison of simulations for the zero-mode modulus as a function of the force F/kT to our uniform approximation, Eq. (C7).

the case. For strong forces, however, the effective modulus is $L\sqrt{fa}/4$ up to some mode number, at which point it crosses over to the previous result.

-
- [1] C. Bustamante, Z. Bryant and S. B. Smith, *Nature* **421**, 423 (2003).
 - [2] A. Ott, M. Magnasco, A. Simon and A. Libchaber, *Phys. Rev. E* **48**, R1642 (1993).
 - [3] F. C. MacKintosh, J. Käs and P. A. Janmey, *Phys. Rev. Lett.* **75**, 4425 (1995).
 - [4] B. Hinner, M. Tempel, E. Sackmann, K. Kroy and E. Frey, *Phys. Rev. Lett.* **81**, 2614 (1998).
 - [5] C. Bustamante, J. F. Marko, E. D. Siggia and S. Smith, *Science* **265**, 1599 (1994).
 - [6] K. Kroy and E. Frey, *Phys. Rev. Lett.* **77**, 306 (1996).
 - [7] J. Wilhelm and E. Frey, *Phys. Rev. Lett.* **77**, 2581 (1996).
 - [8] J. Samuel and S. Sinha, *Phys. Rev. E* **66**, 050801 (2002).
 - [9] A. Dhar and D. Chaudhuri, *Phys. Rev. Lett.* **89**, 065502 (2002).
 - [10] D. A. Kessler and Y. Rabin, *J. Chem. Phys.* **118**, 897 (2003).
 - [11] R. G. Winkler, *J. Chem. Phys.* **118**, 2919 (2003).
 - [12] J. F. Allemand, Ph.D Thesis (Université Pierre et Marie Curie, 1997).
 - [13] Y. Kats, D. A. Kessler and Y. Rabin, *Phys. Rev. E* **65**, 020801(R) (2002).
 - [14] J. F. Marko and E. D. Siggia, *Macromolecules* **27**, 981 (1994).
 - [15] T. Odijk, *Macromolecules* **28**, 7016 (1995).
 - [16] B. Y. Ha and D. Thirumalai, *J. Chem. Phys.* **106**, 4243 (1997).
 - [17] S. V. Panyukov and Y. Rabin, *Phys. Rev. Lett.* **85**, 2404 (2000); *Phys. Rev. E* **62**, 7135 (2000).
 - [18] A. E. H. Love, *A Treatise on the Mathematical Theory of Elasticity* (Dover, New York, 1944).
 - [19] P. G. deGennes, *Scaling Concepts in Polymer Physics* (Cornell University Press, Ithaca, 1979).
 - [20] P. Pincus, *Macromolecules* **10**, 210 (1977).
 - [21] S. V. Panyukov and Y. Rabin, *Phys. Rev. E* **64**, 011911 (2001).
 - [22] D. A. Kessler and Y. Rabin, *Phys. Rev. Lett.* **90**, 024301 (2003).
 - [23] B. Smith, Y. V. Zastavker and G. B. Benedek, *Phys. Rev. Lett.* **87**, 278101 (2001).